J Mater Sci: Mater Med (2007) 18:865–870
DOI 10.1007/s10856-006-0080-3

Electronic states spectroscopy of Hydroxyapatite ceramics

Daniel Aronov · Marina Chaikina · Jehuda Haddad · Anatoly Karlov · Gundars Mezinskis · Leonid Oster · Ilona Pavlovska · Gil Rosenman

Received: 11 April 2005 / Accepted: 22 February 2006 / Published online: 9 January 2007

Abstract Photoluminescence, surface photovoltage spectroscopy and high-resolution characterization methods (Atomic Force Microscopy, Scanning Electron Microscopy, X-ray spectroscopy and DC conductivity) are applied to nanostructured Hydroxyapatite (HAp) bioceramics and allowed to study electron (hole) energy states spectra of the HAp and distinguish bulk and surface localized levels. The measured trap spectra show strong sensitivity to preliminary heat treatment of the ceramics. It is assumed that found deep electron (hole) charged states are responsible for high bioactivity of the HAp nanoceramics.

Introduction

Hydroxyapatite (HAp) is an essential mineral ingredient of bones, tooth and calcified tissues in vertebrate. It has been developed over the past several decades as implantable biocompatible material replacing defective bone tissues. Man-made HAp possesses crystallographic similarity to the biological HAp component and ability to creation a bone-like porous structure [1–7]. Recently applied nanotechnology has allowed fabrication of the HAp ceramics and coatings with particles 15–20 nm for high-strength orthopedic and dental composite [8]. The advantage of the developed HAp is its beneficial biocompatibility and osteoconductivity for bones regeneration and formation of a new bone tissue on their surface without any inclusion [9–11].

Superior HAp bone implants bioactivity is ascribed to high surface area of the nanostructured HAp ceramics [8, 12]. Recent advances in biomaterial research have discovered that the electrically polarized HAp ceramics produces significant biological response [13–15]. It has been demonstrated that the enhanced bone formation is observed at the negatively polarized HAp ceramic surface [16, 17]. The important biological effects are ascribed to high-density stored charges reaching hundreds $\mu C/cm^2$ [14, 18]. The proposed method of polarization is based on bulk electrical polarization of the ceramics induced by applying of external electric field. According to these studies, the tailored electret charge is ascribed to ionic polarization and partly related to migration of protons in the columnar (OH) channels of the HAp [13, 14, 18]. However, a long-term charge storage in dielectric solids may also occur due to electron (hole) trapping at local electronic states in the energy gap resulting in formation of the electret charge [19]. Studies of the trap spectroscopy in the HAp may shed light on microscopic mechanism of these bioceramics interaction with the bone tissue.

D. Aronov · G. Rosenman (✉)
School of Electrical Engineering-Physical Electronics, Tel Aviv University, 69978 Tel Aviv, Israel
e-mail: gilr@eng.tau.ac.il

M. Chaikina · A. Karlov
Center for Orthopedic and Medical Material Sciences of the Siberian Branch of the Russian Academy of Medical Sciences, 634029 Tomsk, Russia

J. Haddad · L. Oster
Sami Shamoon Academic College of Engineering, Beer-Sheva 84100, Israel

G. Mezinskis · I. Pavlovska
Institute of Silicate Materials of the Riga Technical University, Riga, Latvia

In this work, the results of electron states spectroscopy of the nanostructured HAp bioceramics are presented. Combination of photoluminescence and surface photovoltage spectroscopy methods allows to obtain detailed electron (hole) trap spectrum of the HAp and distinguish bulk and surface states. Atomic Force Microscopy (AFM), Scanning Electron Microscopy (SEM), X-ray spectroscopy (XPS), X-ray Diffractometry (XRD), Fourier Transform Infrared spectroscopy (FTIR), and DC conductivity are applied to characterize the ceramics.

HAp ceramics fabrication

HAp nanopowder was fabricated by several steps using both fine mechanic treatment and chemical reactions. Mechanical activation was performed under air environment in a planetary mill containing two steel drums and steel balls. The nanocomposite particles were tested by means of XRD, FTIR spectroscopy and the specific surface analysis. Sizes of particles were defined by means of Transmission Electron Microscopy (TEM). The obtained data show, that all probes are enough crystallized HAp in the form of nanoparticles with sizes being in range from 20 to 100 nm. Particles of typical 40 nm size were extracted for the ceramics manufacturing and used as a raw material for preparation of ceramic platelets.

Two sorts of the HAp nanopowder, ''*A*'' and ''*P*'', were used for the ceramic samples fabrication. The HAp powder ''*P*'' was annealed at 900°C in 2 h and then dispersed in alcohol in 2 min, whilst the powder ''*A*'' was not subjected to any thermal treatment. Such a preliminary high temperature treatment of the powder ''*P*'' should lead to a strong dehydration of the HAp, which was confirmed by subsequent XPS analysis of the HAp ceramics samples. The platelet-like samples (height of 2–3 mm, diameter of 5 mm) were fabricated using dry pressing of the HAp powders (weight of 0.1 ± 0.005 g). A press form greased by rapeseed oil was used for two stage compaction. Pressure of 250 MPa and 375 MPa during the first stage and second one was applied. After pressing the resulting ceramic bodies were sintered with heating rate of 5°C/min up to 1,100°C, followed by annealing at that temperature for 1 h. Sintered platelets were cooled down to room temperature within an oven. The XRD analysis and FTIR spectra of the synthesized samples show the good formed crystalline structure of HAp.

Characterization methods

High-resolution XPS analysis was applied to characterize a chemical composition of the HAp ceramics. The measurements were performed in UHV (3×10^{-10} Torr pressure) using 5600 Multi-Technique System (PHI, USA). The samples were irradiated with a monochromatic Al K_α source (1486.6 eV) and the outcome electrons were analyzed by a Spherical Capacitor Analyzer using the slit aperture of 800 μm. Topography features were observed by AFM (Multimode; Digital Instruments) in tapping mode and were also imaged by SEM using a Raith 150 Ultra High Resolution E-Beam Tool (Raith; GmbH Germany). Additionally, the roughness and the porosity analysis were performed using a WSxM 4.0 Develop 6.1 scanning probe microscopy software from Nanotec Electronica S.L. DC conductivity measurements were conducted by a HP-4339 High Resistance Meter in conjunction with a HP-4284 Precision LCR Meter, which cover the regions of 20 Hz to 1 MHz.

Optical absorption spectra were measured with a Genesis-5 spectrophotometer (Milton Roy, USA) equipped with a PC-IBM. Photoluminescence (PL) excitation and emission spectra were measured with a FP-6200 (Jasco, Japan) spectrofluorometer supported by a Pentium 4 computer. The system employs high quality components designed around a DC powered 150 W Xenon lamp. The lamp output is monitored and maximum stability is ensured by the use of a reference silicon photodiode. The signal-to-noise ratio of the instrument is around 450:1. The wavelength range provided by the FP-6200 is 200–800 nm (excitation) and 200–900 nm (emission) with a WRE-362 red sensitive photomultiplier. Appropriate Long Pass and Cut Off optical filters were applied in order to exclude stray light and second-order effects.

The PL excitation bands were resolved into individual Gaussian components using equation:

$$I = I_{\max}\exp\left[-\left(\frac{\hbar\omega - \hbar\omega_0}{2\sigma^2}\right)^2\right] \quad (1)$$

where I is the PL intensity at photon energy $\hbar\omega$, $I_{\max}$ is the maximum intensity of the individual band, $\hbar\omega_0$ is the exciting photon energy at $I_{\max}$, σ is the band width connected with the FWHM by equation:

$$\mathrm{FWHM} = 2\ln(2)^{1/2}\sigma \quad (2)$$

The ''Peak-Fit'' deconvolution program uses the least square LMM method with simultaneous variation of all or some of the excitation bands parameters (photon energy or alternately—band energy, FWHM, PL intensity) together with fitting baseline to obtain the minimum chi-square.

Surface Photovoltage Spectroscopy (SPS) studies are based on a Kelvin probe technique [20, 21], which measures a contact potential difference (CPD) between a vibrating reference probe and a sample surface subjected to a light illumination. Illumination of the sample surface by monochromatic light results in direct modification of the surface charge, and hence potential that occurs due to photogeneration and separation of the charged carriers. Therefore, the obtained photo-induced variation of ΔCPD spectrum contains information about semiconductor type of conductivity, electron affinity, band gap local states and built-in potentials. It should be noted that a great advantage of SPS compared to PL optical method is an opportunity to distinguish between electron and hole traps by estimation of absolute position of a localized state [22].

SPS measurements were performed in air using a commercial Kelvin probe arrangement (Besocke Delta Phi, Jülich, Germany) with sensitivity of ~1 meV. The vibrating metallic probe consisted of a 2.5 mm diameter semitransparent gold grid mounted at a piezoelectric actuator. The probe was placed in close proximity to the ceramic sample surface. The piezoelectric crystal was moved by an external oscillator at a frequency of 170 Hz. The sample was illuminated by a 250 W tungsten–halogen lamp using a grating monochromator (Jarrell Ash). A value of the CPD and its changes with photon energy were measured using lock-in amplifier and were processed by a Pentium 3 computer.

Results and discussion

Figure 1 illustrates AFM image of the HAp ceramics topography. The both sorts of the prepared ceramics, ''*A*'' and ''*P*'', show identical topographic features. Statistical analysis gave the average size of the ceramic grains around 300 nm and dispersion of 100 nm. The porosity of the fabricated samples characterized by the use of scanning probe microscopy software was around 20%. No difference was found between the ''*A*'' and ''*P*'' ceramic samples in dc conductivity measurements, which showed the value around 10^{-8} 1/(Ω cm).

Composition and atomic concentrations of the elements contained in the investigated ceramics were determined from XPS measurements. The results are shown in Table 1. A typical formula for the HAp is $Ca_{10-x}(HPO_4)_x(PO_4)_{6-x}(OH)_{2-x}$, where X ranges from 0 to 2, giving a Ca/P atomic ratio of between 1.67 and 1.33 [23]. The Ca/P molar ratio of the studied ceramics obtained from XPS measurements was found 1.31 (''*A*'') and 1.54 (''*P*'') and it is related to low stoichiometry composition. Such a difference may be ascribed by some impurities like Na, Mg and Ba at the level about 1%, which were found in the sample ''*A*'' and not resolved in the sample ''*P*''. The pronounced composition difference observed in the ''*A*'' and ''*P*'' ceramic samples was a concentration of hydroxyl-ions $(OH)^-$. It was found that $(OH)^-$ concentration in the ''*A*'' samples larger by 3.5 times than those in the ''*P*''. It might be ascribed to high preliminary heat treatment of the HAp sample ''*P*''.

The measurements of absorption spectra from the HAp were very problematic since the samples are non-transparent and represent strongly dispersed media. However, significant dispersion increasing (relative to the air) observed at the level of photon energy higher

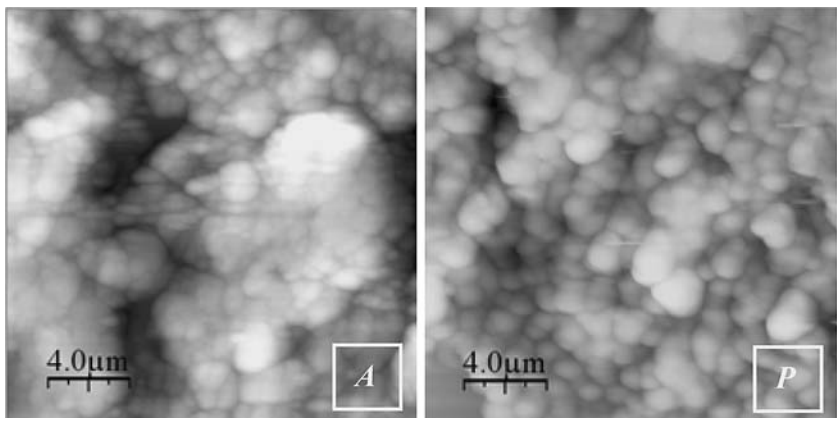

Fig. 1 Atomic Force Microscopy image of Hydroxyapatite ceramics

Table 1 X-Ray photoelectron spectroscopy analysis of Hydroxyapatite ceramics

Sample type	C1s (%)	O1s (%)	Na1s (%)	Mg1s (%)	P2p (%)	Ca2p (%)	Ba3d5 (%)	Si2p (%)	Pb4f7 (%)		Ca:P ratio	$(OH)_x$
A	15.61	52.10	1.55	1.09	10.44	14.00	0.31	–	–	=>	1.31	$x = 3.41$
P	16.53	54.05	–	–	10.96	16.88	–	1.55	0.04	=>	1.54	$x = 0.97$

than 3.7 eV might be related to the region of the beginning of fundamental absorption edge.

The basic optical data were measured by means of excitation spectrum of the PL. First, spectral emission region of the PL was evaluated. Excitation of the HAp ceramics by photon energy of 3.44 eV led to a very wide, continuous optical emission PL spectrum with a wide plateau in the range 540–680 nm. The excitation spectra (Fig. 2) were measured in the region 2.5–6.2 eV using emission band 640 ± 5 nm determined from the plateau of the emission spectrum. It should be marked that the both sorts of the samples, ''*A*'' and ''*P*'', show very similar spectra but the intensity of the PL intensities are strongly differed. The continuous increase of the PL intensity is observed starting from the exciting photon energy of ~3.8 eV. This excitation spectrum behavior in this spectrum region is a firm evidence of the fundamental absorption (inter-band transitions). The fitting of the edge of fundamental optical absorption allowed to evaluate the width of the forbidden band, E_g, in the HAp ceramics for the both, ''*A*'' and ''*P*'', samples between $E_g = 3.8$–4.0 eV. The measured spectra (Fig. 2) represent a wide non-symmetric and non-monotonic optical band indicating that number of the localized energy levels of electron-hole origin is responsible for the spectrum. They were resolved into individual Gaussian components. The energies of these components are shown in Table 2. The deconvolution treatment of the experimental data allowed to obtain an exact value of the energy band gap, $E_g = 4.0$ eV. Several individual energy states were also found. They are located in the energy gap in the range 2.6–3.9 eV (Table 2). Both the excitation spectra (Fig. 2) and deconvoluted data (Table 2) showed that the samples ''*A*'' and ''*P*'' have very close values of the energy band and the localized states energies. However, the observed strong difference in the PL intensity indicated to significant difference in the states concentration.

Table 2 Energy structure of electron (hole) states in Hydroxyapatite obtained from photoluminescence excitation spectra

Sample type	E_1 (eV)	E_2 (eV)	E_3 (eV)	E_4 (eV)	E_6 (eV)	E_g (eV)
A	2.6	2.8	3.0	3.2	3.4	4.0
P	2.6	2.9	3.0	3.2	3.4	4.0

Figure 3 shows a light induced variation of the contact potential difference, ΔCPD. The ΔCPD spectra of the both investigated HAp ceramics samples, ''*A*'' and ''*P*'', are identical. Since light illumination typically tends to decrease the surface band-bending, this would result in a positive ΔCPD in P-type samples and a negative ΔCPD in N-type samples. The obtained ΔCPD spectra (Fig. 3) demonstrate a positive sign of the ΔCPD ''knee'' which allows relating the both HAp samples to P-type [22]. Despite of very similar structure of the ΔCPD spectra a pronounced difference was found for absolute values of the ΔCPD, which is by 10 times higher for the ''*P*'' sample (Fig. 3).

Another basic application of SPS is measurements of a sample band gap E_g and an energy position of

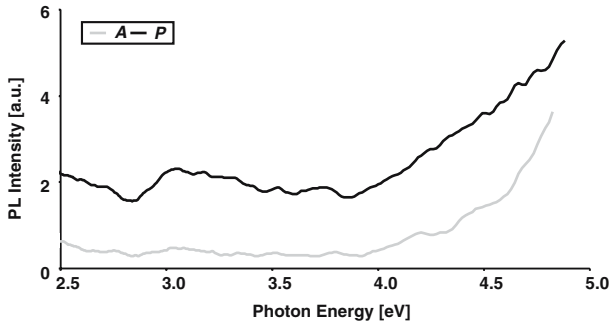

Fig. 2 Photoluminescence excitation spectra from Hydroxyapatite ceramic samples without (''*A*'') and after (''*P*'') thermal treatment

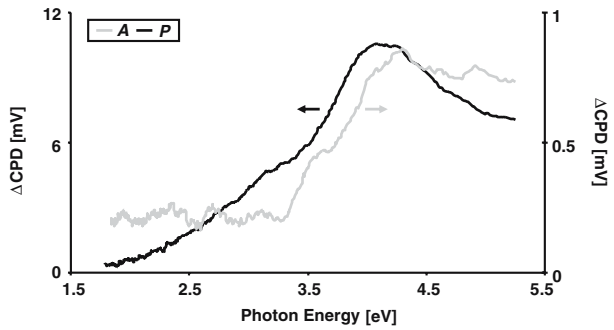

Fig. 3 Surface Photovoltage spectra of Hydroxyapatite ceramic samples without (''*A*'') and after (''*P*'') thermal treatment

localized states. Strong monotonic variation of the ΔCPD (Fig. 3) occurs due to increase of light absorption coefficient near the band gap energy edge which is observed around 3.6–4.0 eV. According to the developed technique of the ΔCPD curves treatment [22] the sharpest change in the slope of the ΔCPD (Fig. 3) is related to the region of the fundamental light absorption. As a result the value of the energy gap in the HAp was determined as $E_g = 3.9$ eV (Table 2), which is consistent with E_g value obtained from the PL data (Fig. 2, Table 2) and theoretical calculations [24].

Identical approach [22] was applied to estimate the energy positions of bulk and surface electron (hole) states. Excitation of electrons from bulk or surface states to the conduction band contributes to a positive change in the surface charge and hence a negative ΔCPD was expected. Conversely, excitation of holes to the valence band makes the surface charge more negative and positive ΔCPD should be observed. The combination of the ΔCPD threshold energy and the slope sign allows finding the absolute energy positions of bulk and surface states. They are determined as tangents intersection of a slope change points at the ΔCPD curves [22]. Table 3 concentrates the estimated bulk and surface states energies for the both HAp samples that were obtained from the ΔCPD data (Fig. 3). The found energy of six localized states is in the range 2.6–3.3 eV. Application of the technique [22] enabled to relate three of them to hole centers and another three to electron ones (Table 4).

Comparison between the ΔCPD (Fig. 3, Table 3) and the PL spectra (Fig. 2, Table 2) indicates that the energy spectra of electron-hole levels studied by two different experimental spectroscopy techniques are very similar (Tables 2, 3). However the electron state $E_5 = 3.3$ eV founded by SPS method was not observed in the PL spectrum. The CPD generated between the Kelvin probe and illuminated sample surface affected both by the surface and near surface-bulk states. However, the PL intensity totally depends on the number of states participating in recombination process resulting in photon emission. The PL is mainly contributed by bulk states. It allows relating the electron state E_5 to the surface state, which does not contribute sufficiently to the PL. Figure 4 demonstrates energy structure of the studied HAp ceramics.

Comparison of the PL and SPS experimental spectroscopy data (Figs. 2, 3, Tables 2, 3) enables to conclude that the both, "*P*" and "*A*", HAp samples have identical electron-hole states structures where five bulk states E_1, E_2, E_3, E_4 and E_6 and one surface state E_5 (Fig. 4, Table 4). However, the observed one order of magnitude variation of the ΔCPD between the two, "*A*" and "*P*", HAp samples (Fig. 3) indicates to a strong difference in elementary defects responsible for the found electron-hole energy state structure. Specifically, preliminary performed thermal treatment of the "*P*" powder led to a higher density of defect concentration compared to the "*A*". They might be $(OH)^-$ vacancies which high concentration was found in the "*P*" samples.

It should be noted that the both sorts of the observed energy states (electron and hole) are deeply located in the energy band. Such energy positions of the localized levels are the basis for the long-term charge retention and formation of a stable electret state, which may be responsible for unconventional biocompatibility of the HAp ceramics.

Table 3 Energy structure of electron (hole) states in Hydroxyapatite measured by surface photovoltage spectroscopy method

Sample type	E_1 (eV)	E_2 (eV)	E_3 (eV)	E_4 (eV)	E_5 (eV)	E_6 (eV)	E_g (eV)
A	2.6	2.8	3.0	3.2	3.3	3.4	3.9
P	2.6	2.9	3.0	3.2	3.3	3.4	3.9

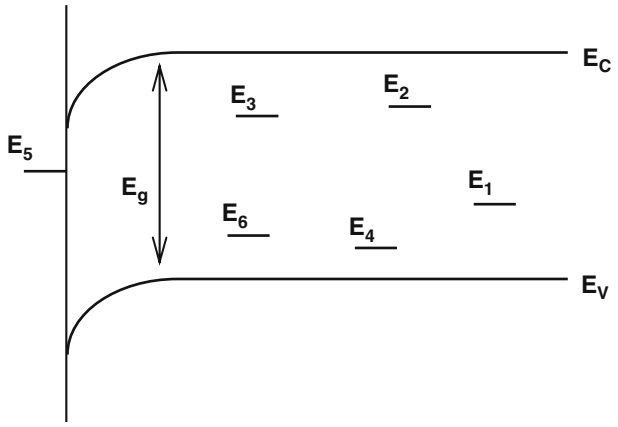

Fig. 4 Band diagram of both ("*A*" and "*P*") Hydroxyapatite ceramics. Where E_1–E_4 and E_6 are the bulk states, E_5 are the surface state and E_g is the bangap energy

Table 4 Energy positions of localized states in Hydroxyapatite

Sample type	E_1 (eV)	E_2 (eV)	E_3 (eV)	E_4 (eV)	E_5 (eV)	E_6 (eV)
A	$E_C - 2.6$	$E_V + 2.8$	$E_V + 3.0$	$E_C - 3.2$	$E_V + 3.3$	$E_C - 3.4$
P	$E_C - 2.6$	$E_V + 2.9$	$E_V + 3.0$	$E_C - 3.2$	$E_V + 3.3$	$E_C - 3.4$

Conclusions

Studies of optical absorption, photoluminescence and surface photovoltage phenomena of the nanostructured HAp bioceramics combining with some high-resolution characterization methods have allowed to find its basic electronic parameters such as energy band and fine electron-hole energy structure. It is assumed that the charged deep localized energy states are responsible for high bioactivity of the HAp ceramics.

Acknowledgment The authors appreciate support of European Commission PROJECT NMP3-CT-504937 *''PERCERAMICS''*

References

1. M. JARCHO, *Clin. Orthop.* **157** (1981) 259
2. D. F. WILLIAMS, in ''Advances in biomaterials'', edited by C. De PUTTER, G. L. De LANGE, K. De GROOT, and A. J. C. LEE (vol. 8, Elsevier Science, Amsterdam, 1988) p. 11
3. J. F. OSBORN, in ''Biomaterials degradation'', edited by M. A. BARBOSA (Elsevier Science, Amsterdam, 1991) p. 185
4. M. NEO, S. KOTANI, Y. FUJITA, T. NAKAMURA, T. YAMAMURO, Y. BANDO, C. OHTSUKI and T. KOKUO, *J. Biomed. Mater. Res.* **26** (1992) 255
5. P. LI and P. DUCHEYNE, *J. Biomed. Mater. Res.* **41** (1998) 341
6. K. DE GROOT, J. G. C. WOLKE and J. A. JANSEN, *J. Eng. Med.* **212** (1998) 137
7. K. DE GROOT, *Biomaterials* **1** (1980) 47
8. B. BEN NISSAN, *MRS Bull.* **29** (2004) 28
9. L. L. HENCH, *J. Am. Ceram. Soc.* **81** (1998) 1705
10. R. H. DOREMUS, *J. Mater. Sci.* **27** (1992) 285
11. J. M. GOMEZ-VEGA, E. SAIZ, A. P. TOMSIA, G. W. MARSHALL and S. J. MARSHALL, *Biomaterials* **21** (2000) 105
12. A. KARLOV and V. SHAKHOV, Russian Federation Patent **2156325** (2000)
13. K. YAMASHITA, K. KITAGAKI and T. UMEGAKI, *J. Am. Ceram. Soc.* **78** (1995) 1191
14. S. NAKAMURA, H. TAKEDA and K. YAMASHITA, *J. Appl. Phys.* **89** (2001) 5386
15. K. YAMASHITA, N. OIKAWA and T. UMEGAKI, *Chem. Mater.* **8** (1996) 2697
16. T. KOBAYASHI, S. NAKAMURA and K. YAMASHITA, *J. Biomed. Mater. Res.* **57** (2001) 477
17. M. OHGAKI, S. NAKAMURA and K. YAMASHITA, in ''Bioceramics'', edited by H. OHGUSHI, G. W. HASTINGS and T. YOSHIKAWA (vol. 12, World Scientific, Singapore, 1999) p. 187
18. M. UESHIMA, S. NAKAMURA and K. YAMASHITA, *Adv. Mater.* **14** (2002) 591
19. G. SESSLER, ''Electrets'' (Springer-Verlag, Berlin, 1980)
20. N. A. SURPLICE and R. J. D'ARCY, *J. Phys. E Sci. Instrum.* **3** (1970) 477
21. J. LAGOWSKI, C. L. BALESTRA and H. C. GATOS, *Surf. Sci.* **29** (1972) 213
22. L. KRONIK and Y. SHAPIRA, *Surf. Sci. Rep.* **37** (1999) 5
23. A. S. POSNER, *Physiol. Rev.* **49** (1969) 760
24. P. RULIS, L. OUYANG and W. Y. CHING, *Phys. Rev.* **B70** (2004) 155104